Highly efficient fluorescence of a fluorescing nanoparticle with a silver shell

Xue-Wen Chen,[1, 2] Wallace C. H. Choy,[1*] Sailing He,[2] and P. C. Chui[1]

[1] *Department of Electrical and Electronic Engineering, University of Hong Kong, Pokfulam Road, Hong Kong, China.*

[2] *Centre for Optical and Electromagnetic Research, Zhejiang University; Joint Research Centre of Photonics of the Royal Institute of Technology (Sweden) and Zhejiang University, Zhijingang campus, Hangzhou 310058, China.*

**Corresponding author: chchoy@eee.hku.hk*

Abstract: Spontaneous emission (SE) rate and the fluorescence efficiency of a bare fluorescing nanoparticle and the nanoparticle with a silver nanoshell are analyzed rigorously by using a classical electromagnetic approach with the consideration of the nonlocal effect of the silver nano-shell. The dependences of the SE rate and the fluorescence efficiency on the core-shell structure are carefully studied and the physical interpretations of the results are addressed. The results show that the SE rate of a bare nanoparticle is much slower than that in the infinite medium by almost an order of magnitude and consequently the fluorescence efficiency is usually low. However, by encapsulating the nanoparticle with a silver shell, highly efficient fluorescence can be achieved as a result of a large Purcell enhancement and high out-coupling efficiency for a well-designed core-shell structure. We also show that a higher SE rate may not offer a larger fluorescence efficiency since the fluorescence efficiency not only depends on the internal quantum yield but also the out-coupling efficiency.

OCIS codes: (300.6280) Spectroscopy, fluorescence and luminescence (240.6680) Surface plasmons (260.2110) Electromagnetic theory

References and links

1. P. N. Prasad, *Introduction to Biophotonics*, (John Wiley & Sons, New York, 2003)
2. F. Wang, W. Tan, Y. Zhang, X. Fan and M. Wang, "Luminescent nanomaterials for biological labeling," Nanotechnology **17**, R1 (2006)
3. R. Y. Tsien, "The green fluorescent protein," Annu. Rev. Biochem. **67**, 509-544 (1998).
4. A. Burns, H. Ow and U. Wiesner, "Fluorescent core–shell silica nanoparticles: towards "Lab on a Particle" architectures for nanobiotechnology," Chem. Soc. Rev. **35**, 1028 (2006).
5. Y. P. Leung, W. C. H. Choy, I. Markov, G. K. H. Pang, H. C. Ong, and T .I. Yuk, "Synthesis of wurtzite ZnSe nanorings by thermal evaporation," Appl. Phys. Lett **88**, 183110 (2006).
6. J. P. Zimmer, S. W. Kim, S. Ohnishi, E. Tanaka, J. V. Frangioni, and M. G. Bawendi, "Size series of small indium. arsenide-zinc selenide core-shell nanocrystals and their application to in vivo imaging," J. Am. Chem. Soc. **128**, 2526 (2006).
7. L. P. Balet, S. A. Ivanov, A. Piryantinski, M. Achermann, and V. I. Klimov, "Inverted core/shell nanocrystals continuously tunable between type-I and type-II localization regimes," Nano. Lett. **4**, 1485 (2004).
8. C. Radloff and N. J. Halas, "Plasmonic Response of Concentric Nanoshells," Nano. Lett. **4**, 1323 (2004).
9. S. R. Sershen, S. L. Westcott, J. L. West and N. J. Halas, "An opto-mechanical nanoshell-polymer composite," Appl. Phys. B-Lasers and Optics **73**, 379 (2001).
10. S. J. Oldenburg, R. D. Averitt, S. L. Westcott, and N. J. Halas, "Nanoengineering of optical resonances," Chem. Phys. Lett. **288**, 243 (1998).
11. C. Graf and A. van Blaaderen, "Metallodielectric colloidal core-shell particles for photonic applications," Langmuir **18**, 524 (2002).
12. M. A. Hines and P. Guyot-Sionest, "Synthesis and characterization of strong luminescing ZnS-capped CdSe nanocrystals," J. Phys. Chem. **100**, 468 (1996).
13. S. Haubold, M. Haase, A. Kornowski and H. Weller, "Strongly luminescent InP/ZnS core-shell nanoparticles," Chemphyschem **2**, 331 (2001).

#82976 - $15.00 USD Received 11 May 2007; revised 18 May 2007; accepted 18 May 2007; published 24 May 2007

14. N. Gaponik, D. V. Talapin, A. L. Rogach, K. Hoppe, E. V. Shevchenko, A. Kornowski, A. Eychmuller and H. Weller, "Thiol-Capping of CdTe nanocrystals:an alternative to organometallic synthetic routes," J. Phys. Chem. B **106**, 7177 (2002).
15. J. R. Lakowicz, "Radiative Decay Engineering: Biophysical and Biomedical Applications," Anal.Biochem. **298**, 1 (2001).
16. E. M. Purcell, "Spontaneous emission probabilities at radio frequencies," Phys. Rev. **69**, 681 (1946).
17. W. Lukosz, ''Theory of optical-environment-dependent spontaneous emission rates for emitters in thin layers,''Phys. Rev. B **22**, 3030 (1980).
18. K. Okamoto, I. Niki, A. Shvartser, Y. Narukawa, T. Mukai, and A. Scherer, "Surface-plasmon-enhanced light emitters based on InGaN quantum wells," Nat. Mater. **3**, 601(2004).
19. A. Moroz, "Spectroscopic properties of a two-level atom interacting with a complex spherical nanoshell," Chem. Phys. **317**, 1(2005).
20. J. Enderlein, "Theoretical study of single molecule fluorescence in a metallic nanocavity,"Appl. Phys. Lett. **80,** 315 (2002).
21. X. W. Chen, W. C. H. Choy, S. He and P. C. Chui, "Accurate analysis and optimal design of top-emitting organic light emitting devices," J. Appl. Phys. (in press).
22. A. R. Melnyk and M. J. Harrison,"Theory of optical excitation of plasmons in metals," Phys. Rev. B **2**, 835 (1970).
23. P. T. Leung, "Decay of molecules at spherical surfaces: nonlocal effects," Phys. Rev. B **42**, 7622 (1990).
24. A. Pack, M. Hietschold, and R. Wannemacher, "Failure of local Mie theory: optical spectra of colloidal aggregates," Opt. Commun. **194**, 277 (2001).
25. R. K. Lee, Y. Xu, and A. Yariv, "Modified spontaneous emission from a two dimensional photonic bandgap crystal slab, " J. Opt. Soc. Am. B **17**, 1438 (2000).
26. H. Chew, "Radiation and lifetime of atoms inside dielectric particles," Phys. Rev. A **38**, 3410 (1988).
27. A. Moroz, "A recursive transfer-matrix solution for a dipole radiating inside and outside a stratified sphere," Anna. Phys. **315**, 352 (2005).
28. K. Neyts, "Simulation of light emission from thin-film microcavities," J. Opt. Soc. Am. A **15**, 962 (1998).
29. W. C. Chew, *Waves and Fields in Inhomogeneous Media* (IEEE Press, New York, 1995), Chap. 3.
30. L. Kuipers and R. Timman, *Handbook of Mathematics* (Pergamon Press, 1969).
31. J. Enderlein, "Response to comments on "theoretical study of single molecule fluorescence in a metallic nanocavity," Appl. Phys. Lett. **87**, 066102 (2005).
32. E. D, Palik, *Handbook of Optical Constants of Solids* (Academic press, Boston, 1985).
33. A. Taflove, *Computational Electrodynamics: The Finite-Difference Time-Domain Method* (Artech House INC,Norwood, 2000), 2nd ed.

1. Introduction

Fluorescent nanomaterials, including organic and metallorganic dye molecules, fluorescent proteins, II-VI and III-V compound semiconductor nanoparticles, polymer/dye-based nanoparticles and silica/dye hybrid particles, have been the subject of intensive research in recent years for their vast applications ranging from biomedical therapeutics and diagnostics to information storage and optoelectronics [1-9]. A wide range of physical and chemical methods has been developed for the synthesis of nanoparticles and nanoscale core-shell structures with controllable core radius and shell thicknesses [10,11]. For fluorescence based applications, fluorescence efficiency, i.e. the external quantum efficiency (η_{ext}) of the emitter, is an important issue. Due to the existence of pronounced nonradiative decay of excitons in the nanoscale structure, low η_{ext} is an often-observed feature. Most of the strategies so far employed aim to reduce the nonradiative decay rate [12-14] for improving the fluorescence efficiency. The direct and effective approach to improve η_{ext} is to increase radiative decay rate[15] and the out-coupling efficiency since η_{ext} is the product of internal quantum yield (i.e. internal quantum efficiency) and the outcoupling efficiency. The enhancement of radiative decay rate results in the Purcell enhancement of the internal quantum yield [16,17]. However, there are few studies on increasing the radiative decay rate and out-coupling efficiency simultaneously in core-shell nanoparticles to enhance the fluorescence efficiency. Here, we will address this issue.

The radiative decay rate, i.e. spontaneous emission (SE) rate, can be enhanced by utilizing the surface plasmon effect [18-20] or the microcavity effect [21]. According to the near field nature of surface plasmon, the SE rate in a dielectric nanoparticle encapsulated with a metallic

#82976 - $15.00 USD Received 11 May 2007; revised 18 May 2007; accepted 18 May 2007; published 24 May 2007

shell can be greatly enhanced. However, the metallic shell introduces extra absorption loss and may result in a small outcoupling efficiency. Consequently, fluorescence efficiency may still be low although the SE rate is greatly enhanced. Thus a rigorous theoretical study on the SE rate and the out-coupling efficiency of emitters in nanoscale structure is desirable for getting a better physical understanding and optimal design of the nano-structure to achieve high-efficiency fluorescence. In this paper, the SE rates and η_{ext} of emitters in a spherical nanofluorophore with and without a silver nanoshell are rigorously investigated through a classical electromagnetic approach with the consideration of the nonlocal effect of the silver nanoshell [22-23]. In the presence of silver nano-shell, the standard Mie theory may fail since the nonlocal effects come into play due to the excitation of longitudinal surface plasmon modes [24]. The applicability of the classical electromagnetics for calculating the radiative decay rate relies on the fact that the local photonic density of states also describes the averaged total power emitted from the incoherent classical electric dipoles [25].

Different from the SE rate in a dielectric particle with a diameter around several wavelengths [26], the SE rate in a nanoparticle with a diameter below 100nm is considerably slower than that in free space by almost an order of magnitude. Our results show that the fluorescence of a bare nanoparticle is inefficient since nonradiative decay outweighs radiative decay. By encapsulating the nanoparticle with a silver nano-shell, the SE rate can be enhanced by orders of magnitude due to the resonant excitation of surface plasmons. However, our results also show that the out-coupling efficiency is usually low for very high SE rate.

The paper is organized as follows. In Section II, we formulate a general approach to calculate the SE rate and η_{ext} of emitters in a spherically multilayered structure with arbitrary permittivity. Our approach which directly relates the SE rate to the imaginary part of the electric field at the dipole position is convenient for implementation and more general as compared with the scheme employed in Ref. [27], where the calculation becomes complicated when the number of lossy shells increases. In Section III, the SE rate and η_{ext} of a nanoparticle with and without a silver nanoshell of various core radii and shell thicknesses are studied and the physical explanations of the results are given. We present concluding remarks in section IV.

2. Theory

In this section, we will present a generalized theoretical analysis of SE in a spherically multilayered structure of arbitrary permittivity and number of shells. The structure and parameters of a multilayered sphere are displayed on Fig. 1. An emitting shell is sandwiched between two stacks of shells, i.e., P outer shells and Q inner shells. The relative permittivity and the boundary of the i^{th} shell are denoted as ε_i (i = –Q,…,P) and r_{i+1} (i = –Q,…, P-1), respectively. The emitting medium is assumed to be non-absorbing at the emitting wavelength while the other shells can be either transparent or absorptive, including metallic shells. As mentioned previously, the quantum emitter can be modeled as incoherent classical electric dipoles (with a constant current but random orientation in space). The SE properties of the emitter can be characterized by using the averaged total radiation power *F* and the power radiated to farfield *U* (normalized by the total radiation power of an electric dipole in infinite medium) of the dipoles in the spherically multilayered structure. As a consequence of Fermi's golden rule, the radiative decay rate is optical-environment-dependent as [17, 28]

$$\Gamma_r^s = F \cdot \Gamma_r^0 \tag{1}$$

where Γ_r^0 and Γ_r^s are the exciton radiative decay rate in free space and spherically multilayered media, respectively.

#82976 - $15.00 USD Received 11 May 2007; revised 18 May 2007; accepted 18 May 2007; published 24 May 2007

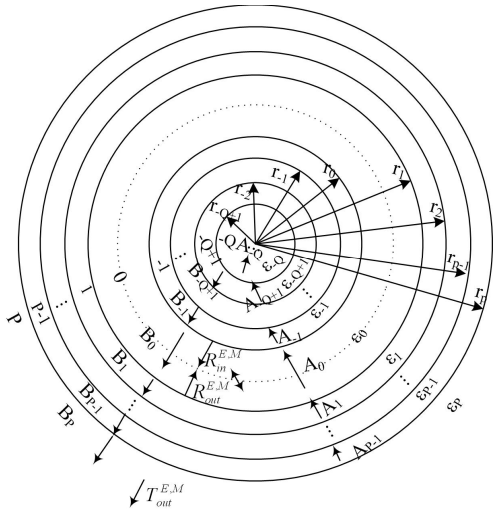

Fig. 1 Geometry and parameters of a spherically multilayered structure with Q layers below and P layers above the 0th shell where an electric dipole is located. r_i (i=-Q+1,…,P) denotes the position of the i^{th} boundary; ε_i, A_i and B_i (i=-Q,…,P) denote the relative permittivity, decomposition coefficients of the inward and outward waves, respectively; $R_{out,l}^{E/M}$, $R_{in,l}^{E/M}$ and $T_{out,l}^{E/M}$ are the total reflection coefficient from the outer shells, the total reflection coefficient from the inner shells and the total transmission coefficient of TE/TM polarization, respectively.

The averaged total radiation power *F*, also called as the Purcell factor, can be considered as a normalized SE rate. The change of radiative decay rate will result in the change of the internal quantum yield (internal quantum efficiency) since the radiative and non-radiative recombinations are competing processes. Assuming that the non-radiative decay rate in the spherically multilayered structure is Γ_{nr}, the internal quantum yield in the spherically multilayered media η_q^s is modified as

$$\eta_q^s \equiv \frac{\Gamma_r^s}{\Gamma_r^s + \Gamma_{nr}} = \frac{F}{F\eta_q^0 + \left(1-\eta_q^0\right)} \cdot \eta_q^0 \tag{2}$$

where η_q^0 is the initial internal quantum yield when *F*=1. η_{ext} is given by

$$\eta_{ext} \equiv \eta_q^s \cdot \frac{U}{F} = \frac{U}{F\eta_q^0 + \left(1-\eta_q^0\right)} \cdot \eta_q^0 \tag{3}.$$

In the infinite medium of ε_0, the electric field at $\vec{r}$ induced by a dipole source at $\vec{r}'$ with an arbitrary orientation $\vec{\rho}$ and dipole moment Θ is given as

$$E^0\left(\vec{r},\vec{r}'\right) = \left(\vec{\vec{I}} + \frac{\nabla\nabla}{k_0^2}\right) \cdot \vec{\rho}\Theta \frac{e^{ik_0\left|\vec{r}-\vec{r}'\right|}}{4\pi\left|\vec{r}-\vec{r}'\right|} \tag{4},$$

where $\vec{\vec{I}}$ is the unitary dyadic and k_0 is the wavenumber in the emitting medium. In the spherically multilayered media, the electric field is modified as

$$E^S = E^0 + E_{\vec{\rho}}^r \tag{5}.$$

#82976 - $15.00 USD Received 11 May 2007; revised 18 May 2007; accepted 18 May 2007; published 24 May 2007

where $E^r_{\vec{\rho}}$ is the total reflected field from the outer and inner interfaces. Then the total radiation power for a dipole with orientation $\vec{\rho}$ can be obtained by[17]

$$F = 1 + \frac{6\pi}{k_0\Theta}\vec{\rho}\cdot\Im\left(E^r_{\vec{\rho}}(\vec{r}',\vec{r}')\right) \tag{6}$$

where $\Im(\cdot)$ stands for the imaginary part of $(\cdot)$. For incoherent dipoles with random orientations, the averaged total radiation power is

$$F = 1 + \frac{2\pi}{k_0\Theta}\left[\vec{\gamma}\cdot\Im\left(E^r_{\vec{\gamma}}(\vec{r}',\vec{r}')\right) + \vec{\theta}\cdot\Im\left(E^r_{\vec{\theta}}(\vec{r}',\vec{r}')\right) + \vec{\phi}\cdot\Im\left(E^r_{\vec{\phi}}(\vec{r}',\vec{r}')\right)\right] \tag{7}$$

where $\vec{\gamma},\vec{\theta}$ and $\vec{\phi}$ are the unit vectors in spherical coordinates. To calculate the reflected electric field and the electric field outside the sphere, we decompose $E^0(\vec{r},\vec{r}')$ in terms of vector spherical harmonics with TM and TE polarizations (with respect to the radical coordinate) as [29]

$$E^0(\vec{r},\vec{r}') = \sum_{l=1}^{\infty}\sum_{m=-l}^{l}\left(\frac{i\alpha^E_{lm}}{\sqrt{l(l+1)}} - \frac{\alpha^M_{lm}}{\omega\varepsilon\varepsilon_0\sqrt{l(l+1)}}\nabla\times\right)\nabla\times\left(\vec{r}h^{(1)}_l(k_0|\vec{r}|)Y_{lm}(\theta,\phi)\right) \text{ for } \left(|\vec{r}|>|\vec{r}'|\right) \tag{8.a}$$

$$E^0(\vec{r},\vec{r}') = \sum_{l=1}^{\infty}\sum_{m=-l}^{l}\left(\frac{i\beta^E_{lm}}{\sqrt{l(l+1)}} - \frac{\beta^M_{lm}}{\omega\varepsilon\varepsilon_0\sqrt{l(l+1)}}\nabla\times\right)\nabla\times\left(\vec{r}j_l(k_0|\vec{r}|)Y_{lm}(\theta,\phi)\right) \text{ for } \left(|\vec{r}|<|\vec{r}'|\right) \tag{8.b}$$

where

$$\alpha^E_{lm} = ik_0\Theta\vec{\rho}\cdot\left(\nabla'\times\vec{r}'\, j_l(k_0|\vec{r}'|)\left(\frac{iY_{lm}(\theta',\phi')}{\sqrt{l(l+1)}}\right)^*\right), \tag{9.a}$$

$$\alpha^M_{lm} = \frac{k_0}{\omega\mu}\Theta\vec{\rho}\cdot\left(\nabla'\times\nabla'\times\vec{r}'\, j_l(k_0|\vec{r}'|)\left(\frac{iY_{lm}(\theta',\phi')}{\sqrt{l(l+1)}}\right)^*\right) \tag{9.b}$$

$$\beta^E_{lm} = ik_0\Theta\vec{\rho}\cdot\left(\nabla'\times\vec{r}'\, h^{(1)}_l(k_0|\vec{r}'|)\left(\frac{iY_{lm}(\theta',\phi')}{\sqrt{l(l+1)}}\right)^*\right), \tag{9.c}$$

$$\beta^M_{lm} = \frac{k_0}{\omega\mu}\Theta\vec{\rho}\cdot\left(\nabla'\times\nabla'\times\vec{r}'\, h^{(1)}_l(k_0|\vec{r}'|)\left(\frac{iY_{lm}(\theta',\phi')}{\sqrt{l(l+1)}}\right)^*\right) \tag{9.d}$$

Here ω, ε and μ are the angular frequency, permittivity and permeability in vacuum, respectively; j_l, $h^{(1)}_l$ and Y_{lm} are the spherical Bessel function, spherical Hankel function of first kind and the normalized scalar spherical harmonics [30], respectively. The asterisk denotes the complex conjugation and ∇' is an operator acting on the prime coordinates. Since only the electric field in the emitting shell and outside the sphere is of interest, as shown in Fig. 1 the two stacks of shells can be considered as two "black" shells characterized by the total inward reflection coefficient $R^{E/M}_{in,l}$, total outward reflection coefficient $R^{E/M}_{out,l}$ and total transmission coefficient $T^{E/M}_{out,l}$, where the superscript E/M denotes polarization state and the subscript *l* is the order of the spherical harmonics. It should be noted that, in the presence of ultra-thin metallic shells, nonlocal effect due to excitations of longitudinal plasmon modes may come into play [22-24]. Then an additional boundary condition is required to characterize this effect [22-24]. We find that for the cases considered in this paper the nonlocal effect is

#82976 - $15.00 USD Received 11 May 2007; revised 18 May 2007; accepted 18 May 2007; published 24 May 2007

prominent for silver shells thinner than 20 nm. The detailed derivations of total reflection coefficients and transmission coefficient, including the case of the structures with ultra-thin metallic shells, are given in the appendix. The reflected electric field can be obtained as

$$E^r(\vec{r},\vec{r}') = \sum_{l=1}^{\infty}\sum_{m=-l}^{l}\left(\frac{iR_{in,l}^E\left(\alpha_{lm}^E R_{out,l}^E + \beta_{lm}^E\right)}{\left(1-R_{out,l}^E R_{in,l}^E\right)} - \frac{R_{in,l}^M\left(\alpha_{lm}^M R_{out,l}^M + \beta_{lm}^M\right)}{\omega\varepsilon\varepsilon_0\left(1-R_{out,l}^M R_{in,l}^M\right)}\nabla\times\right)\frac{\nabla\times\left(\vec{r}h_l^{(1)}\left(k_0|\vec{r}|\right)Y_{lm}(\theta,\phi)\right)}{\sqrt{l(l+1)}}$$
$$+\sum_{l=1}^{\infty}\sum_{m=-l}^{l}\left(\frac{iR_{out,l}^E\left(\alpha_{lm}^E + R_{in,l}^E\beta_{lm}^E\right)}{\left(1-R_{out,l}^E R_{in,l}^E\right)} - \frac{R_{out,l}^M\left(\alpha_{lm}^M + R_{in,l}^M\beta_{lm}^M\right)}{\omega\varepsilon\varepsilon_0\left(1-R_{out,l}^M R_{in,l}^M\right)}\nabla\times\right)\frac{\nabla\times\left(\vec{r}j_l\left(k_0|\vec{r}|\right)Y_{lm}(\theta,\phi)\right)}{\sqrt{l(l+1)}} \quad (10).$$

The power radiated to far-field can be obtained as [26]

$$U = \sum_{l=1}^{\infty}\sum_{m=-l}^{l}\sqrt{\frac{\varepsilon_0}{\varepsilon_P}}\left(\left|\frac{\left(\alpha_{lm}^E + \beta_{lm}^E R_{in,l}^E\right)T_{out,l}^E}{1-R_{out,l}^E R_{in,l}^E}\right|^2 + \frac{\mu}{\varepsilon\varepsilon_P}\left|\frac{\left(\alpha_{lm}^M + \beta_{lm}^M R_{in,l}^M\right)T_{out,l}^M}{1-R_{out,l}^M R_{in,l}^M}\right|^2\right) \Big/ \left(\left|\alpha_{lm}^E\right|^2 + \frac{\mu}{\varepsilon_0\varepsilon}\left|\alpha_{lm}^M\right|^2\right) \quad (11).$$

Here the medium outside the multilayered structure is assumed to be lossless. Consequently, *F* and *U* can be readily calculated. The convergence of the summations in Eq. (10) and Eq. (11) is fast for the spherically multilayered structure with small size. For all the cases studied in this paper, a relative error below 10^{-5} can be guaranteed when the summations are truncated at l=20. The scheme for calculating *F* here is general regardless of the permittivity of the other shells, while the scheme used in ref. [27] depends on the material of the other shells and becomes increasingly complicated when the number of lossy shells increases.

3. Results and discussion

In this section, the SE properties of emitters in a bare nanoparticle and the nanoparticle with a silver nanoshell are studied and discussed in subsection 3.1 and subsection 3.2, respectively. The dependences of the fluorescence efficiencies on the structural parameters of nanoparticle are investigated for two initial internal quantum yields, i.e. $\eta_q^0 = 0.25$ and $\eta_q^0 = 0.75$. The nanoparticle under study here is a dielectric sphere and its material is not restricted here and in principle can be any type of fluorescent nanomaterials. In the calculation, the refractive index of the nanoparticle is set to be 2.0 over the wavelength of interest. According to Ref. [31] and the references therein, the dielectric function of bulk silver [32] is used in the calculation. For a verification of our model, we also used a three-dimensional finite difference time domain (3D-FDTD) method with a dispersive model of silver [33] to calculate *F* and *U* for a nanoparticle with a radius of 30nm and a silver nanoshell of 19 nm. The results obtained by the two methods agree well. However, the 3D-FDTD method is very time consuming.

3.1 SE in a bare nanoparticle

SE properties of the emitters in a bare spherical nanoparticle with a radius *r* is studied and discussed in this subsection. Figure 2(a) plots the wavelength dependence of the normalized SE rate of emitters located at the center of the nanoparticle with a radius of 20nm. One sees that the SE rate is nearly one tenth of the SE rate in free space and decreases gradually as the wavelength increases. The size dependence of the normalized SE rate at the wavelength of 500nm is shown in Fig. 2(b) as the solid line with filled squares. The SE rate decreases as the radius of the nanoparticle decreases. As the radius further decreases, the SE rate has a limiting value around 0.11. This value depends on the refractive index of the nanoparticle and becomes smaller as the refractive index increases. Figure 2(b) also shows η_{ext} for the cases of $\eta_q^0 = 0.25$ and $\eta_q^0 = 0.75$ at the wavelength of 500nm. Due to the low SE rate (*F*), η_{ext} are much smaller than their initial quantum yields according to Eq. (3) where *U* equals *F* in the case of a bare nanoparticle. The degradation of η_{ext} for $\eta_q^0 = 0.25$ is more pronounced than

#82976 - $15.00 USD Received 11 May 2007; revised 18 May 2007; accepted 18 May 2007; published 24 May 2007

that for $\eta_q^0 = 0.75$. This is because the ratio of radiative decay rate to nonradiative decay rate for $\eta_q^0 = 0.25$ drops faster as *F* decreases. But even for $\eta_q^0 = 0.75$, η_{ext} drops to about 20% at *r* = 20nm. Consequently, a bare nanoparticle usually shows inefficient fluorescence.

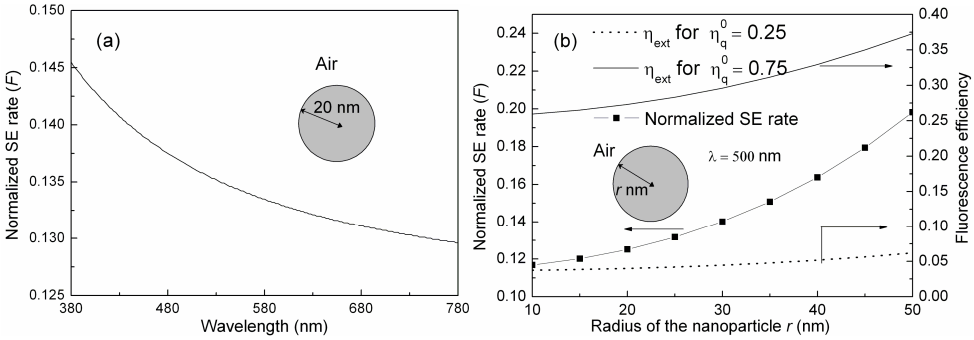

Fig. 2(a). Wavelength dependence of the normalized SE rate for a fixed nanoparticle *r* = 20nm (b) Variance of the normalized SE rate and the fluorescence efficiency for $\eta_q^0 = 0.25$ and $\eta_q^0 = 0.75$ with the increase of the size of the nanoparticle at the wavelength of 500nm.

3.2 SE in the nanoparticle with a silver nanoshell

The SE rate can be greatly enhanced when the nanoparticle is encapsulated with a silver nanoshell due to the resonant excitation of surface plasmons. Unlike the previous case of a bare nanoparticle where *U* equals *F*, *U* is smaller than *F* in the present case since a considerable part of power is absorbed in the silver shell. Thus both *F* and *U* should be calculated for characterizing the SE properties. For the nanoparticle with a silver nano-shell, two parameters, namely, the silver shell thickness *s* and the core radius *r*, can be used to tune the SE properties. Here the SE properties of the emitters centered in the nanoparticle are studied separately for two cases, i.e. (i) the thickness effect of the silver shell and (ii) the size effect of the nanoparticle.

3.3 Case (i): thickness effect of the silver shell

The thickness effect of the silver shell on the SE properties is studied for the silver encapsulated nanoparticle with various shell thickness *s* and a fixed core radius *r* of 30nm as shown in Fig. 3(a). As compared with a bare nanoparticle, the present case shows some remarkable features. First of all, the spectrum of the SE rate shows a resonant structure and the SE rate at the resonant wavelength is several orders of magnitude larger than the SE rate in a bare nanoparticle due to the resonant excitation of surface plasmons.

#82976 - $15.00 USD Received 11 May 2007; revised 18 May 2007; accepted 18 May 2007; published 24 May 2007

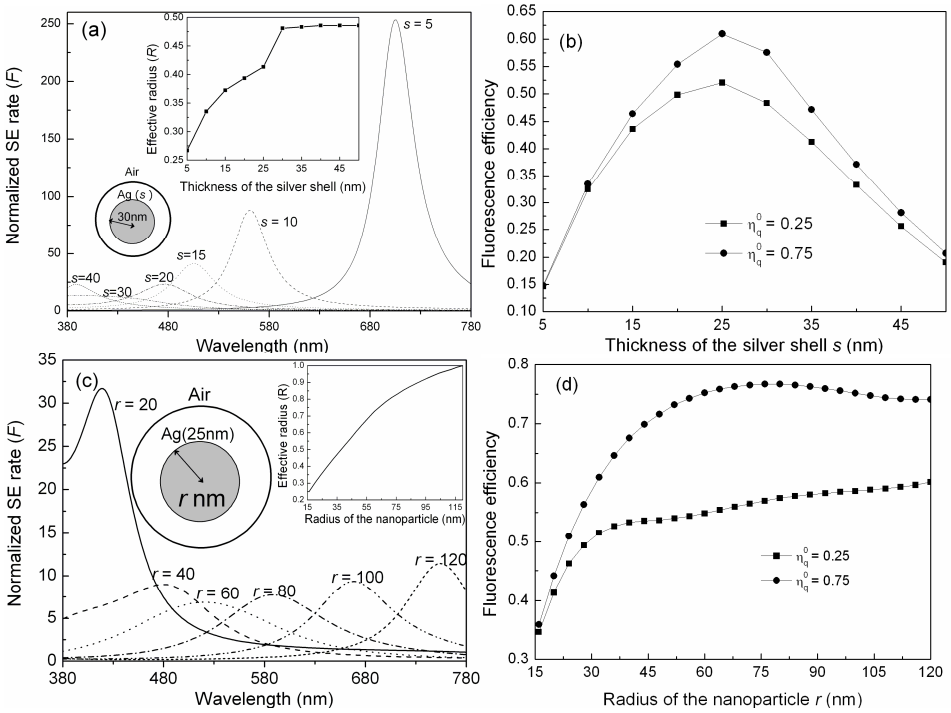

Fig. 3. (a). Wavelength dependence of the normalized SE rate in silver encapsulated nanoparticles of various Ag shell thicknesses *s* (nm) and fixed core radius; inset shows the variance of the effective radius with the increase of the shell thickness. (b) Variance of the fluorescence efficiency with the increase of Ag shell thickness and fixed core radius. (c) Wavelength dependence of the normalized SE rate in silver encapsulated nanoparticles of various core radii *r* (nm) and fixed Ag shell thickness; inset shows the variance of the effective radius with the increase of the core radius (d) Variance of the fluorescence efficiency with the increase of core radius and fixed Ag shell thickness.

The large increment of the SE rate will result in a great enhancement of the internal quantum yield due to the Purcell enhancement according to Eq. (2). Secondly, another distinct feature of Fig. 3(a) is that the resonant wavelength of the spectrum of the SE rate shows a blue shift as *s* increases. For the shells thinner than 5nm, the resonant wavelength shifts out of the visible wavelength range. Meanwhile, for the shells thicker than 30nm, the resonant wavelength shows no obvious shift and the spectrum of the SE rate flattens out as *s* further increases. In addition, the peak value of the normalized SE rate (hereafter named "the peak SE rate") is reduced as *s* increases. To understand the reduction of the peak SE rate, we define an effective radius as $R = 2\pi r/\lambda_r$, where λ_r is the resonant wavelength, to characterize the strength of surface plasmon effects. The surface plasmon effect decreases exponentially as *R* increases. The inset of Fig. 3(a) shows the dependence of the effective radius on the shell thickness. It can be observed that the effective radius firstly increases as *s* increases. Thus in Fig. 3(a) the peak SE rate is reduced and the resonant spectrum broadens as *s* increases from 5nm to 30nm. In another word, the reason why the peak SE rate is larger for thinner silver shell is that the strength of surface plasmon effect is larger since the effective radius *R* is smaller. For thicker silver shell (*s* > 30nm), the microcavity effect of the silver shell gradually dominates and the resonant spectrum sharpens again as *s* further increases.

Figure 3(b) shows the dependence of the fluorescence efficiency at the resonant wavelength on the shell thickness. As compared with Fig. 2(b) for a bare nanoparticle, the fluorescence efficiency of the nanoparticle encapsulated with a suitable thickness of silver

#82976 - $15.00 USD Received 11 May 2007; revised 18 May 2007; accepted 18 May 2007; published 24 May 2007

shell is much larger. Moreover, the fluorescence efficiency for the core-shell structure with *r* = 30nm and *s* = 25nm is much larger than the initial internal quantum yield, particularly for $\eta_q^0 = 0.25$ where a nearly 100% increment is achieved. This is due to a combination of the Purcell enhancement of the internal quantum yield and a high out-coupling efficiency. From Figs. 3(a) and 3(b), one sees that for the nanoparticle with ultra-thin silver shell although the SE rate is very large the fluorescence efficiency is still low since the out-coupling efficiency *U*/*F* is small (e.g. for *s* = 5nm, the fluorescence efficiency is only 0.14.), i.e. most of the emitted power is absorbed in the silver shell. As shown in Fig. 3(b), η_{ext} for the cases of $\eta_q^0 = 0.25$ and $\eta_q^0 = 0.75$ increases as *s* increases from 5nm to 25nm. As *s* further increases fluorescence decreases gradually since the absorption loss in the Ag shell increases again. Consequently, from Figs. 3(a) and 3(b) , one sees that the fluorescence efficiency can be maximized through simultaneously achieving a large Purcell enhancement and high out-coupling efficiency by carefully designing the Ag thickness.

3.4 Case (ii): size effect of the nanoparticle

The size effect of the nanoparticle on the SE properties is studied for the silver encapsulated nanoparticles with various core radii *r* and an optimized shell thickness *s* of 25nm as shown in Fig. 3(c). The resonant wavelength of the SE rate spectrum shows a red-shift as *r* increases. For *r* < 70nm, the peak SE rate in Fig. 3(c) decreases as the radius of the nanoparticle increases. To explain this, the effective radius *R* is calculated and its dependence on the core size is plotted in the inset of Fig. 3(a). We see that even through the resonant wavelength increases with *r*, the effective radius *R* still increases with *r*. In other words, the strength of surface plasmon effect decreases as *r* increases and thus the peak SE rate is reduced and the resonant spectrum is broadened as *r* increases. For *r*>70nm, the microcavity effect of the silver shell gradually goes up and the spectrum of the SE rate becomes narrower and the peak value is increased as *r* increases.

Figure 3(d) plots the size dependence of the fluorescence efficiency for $\eta_q^0 = 0.25$ and $\eta_q^0 = 0.75$ at the resonant wavelength. For r>120nm and r<15nm, the result is not shown here since the resonant wavelength is out of the visible range. As compared with Fig. 2(b), large enhancement of the fluorescence efficiency is obtained due to the Purcell enhancement of the internal quantum yield and a high out-coupling efficiency. For the nanoparticles with a smaller radius although the SE rate is much higher the fluorescence efficiency is low since the out-coupling efficiency *U/F* is low. The fluorescence efficiency at the resonant wavelength increases as the radius of nanoparticle increases.

From the analysis and discussion of the above two cases, we can summarize that highly efficient fluorescence can be achieved in the silver encapsulated nanoparticle through a proper design of the core radius and the shell thickness. The SE rate can be enhanced by several orders of magnitude and the resonant feature of the spectrum of the SE rate depends on the core radius and the shell thickness. It should be noted that a higher SE rate may not give larger fluorescence efficiency since the fluorescence efficiency as given by Eq. (3) not only depends on the quantum yield but also the out-coupling efficiency *U*/*F*. For a fluorescing nanomaterials with specified intrinsic fluorescence spectrum and the initial internal quantum yield, the nanoparticle's radius and thickness of the silver nanoshell should be optimized (simply by scanning the two parameters) to match the spectrum of the SE rate to the intrinsic emission spectrum of the emitter for achieving high-efficiency fluorescence.

4. Conclusion

In this paper, we have formulated a general approach for calculating the SE rate and η_{ext} of the emitters in a spherically multilayered structure with arbitrary permittivity. In the presence of silver nano-shell, nonlocal effect has been taken into account. By using the method, the SE

#82976 - $15.00 USD Received 11 May 2007; revised 18 May 2007; accepted 18 May 2007; published 24 May 2007

rates and fluorescence efficiencies of the emitters in a bare nanoparticle and the nanoparticle with a silver nanoshell are investigated. The SE rate in a bare nanoparticle is only one tenth of the SE rate in free space and consequently the fluorescence is usually inefficient. The SE rate can be enhanced by orders of magnitude through encapsulating the nanoparticle with a silver nanoshell due to the resonant excitation of the surface plasmon. The spontaneous emission properties of the emitters in the nanoparticle with a silver nanoshell are studied separately for two cases, i.e. (i) the size effect of the nanoparticle and (ii) the thickness effect of the silver shell. Through a proper design of the core radius and shell thickness, highly efficient fluorescence can be achieved as a result of the combination of the large Purcell enhancement of quantum yield and a high outcoupling efficiency.

Acknowledgments

We would like to acknowledge the support of UDF grant, the strategic research grant in organic optoelectronics of the University of Hong Kong and the grant (#14300.324.01) from the Research Grant Council of the Hong Kong Special Administrative Region, China.

Appendix

In this appendix, we will show how the total reflection coefficient and transmission coefficient are calculated for a spherically multilayered structure. We first treat the structure consisting of only ordinary shells, i.e. no ultra-thin metallic shells exist, and then the structure including ultra-thin metallic shells. In spherically layered media since TE mode and TM mode are decoupled [29], they can be treated separately. The electric field of TE/TM mode in any shell of the structure can be expressed as the summation of the inward and outward going spherical waves as shown in Fig. 1. For example, in the nth shell, the electric fields of TE and TM modes are

$$E^{TE}(\vec{r}) = \sum_{l=1}^{\infty}\sum_{-l}^{l}\left[\frac{i\nabla\times\vec{r}\left(A_{lm}^{E}(n)\,j_l\left(k_n|\vec{r}|\right)+B_{lm}^{E}(n)\,h_l^{(1)}\left(k_n|\vec{r}|\right)\right)Y_{lm}(\theta,\phi)}{\sqrt{l(l+1)}}\right] \quad \text{(A1) and}$$

$$E^{TM}(\vec{r}) = \sum_{l=1}^{\infty}\sum_{m=-l}^{l}\left(-\frac{\nabla\times\nabla\times\vec{r}\left(A_{lm}^{M}(n)\,j_l\left(k_n|\vec{r}|\right)+B_{lm}^{M}(n)\,h_l^{(1)}\left(k_n|\vec{r}|\right)\right)Y_{lm}(\theta,\phi)}{\omega\varepsilon\varepsilon_n\sqrt{l(l+1)}}\right) \quad \text{(A2)},$$

respectively. Here $A_{lm}^{E/M}$ and $B_{lm}^{E/M}$ are the decomposition coefficients of inward and outward going spherical waves for TE/TM mode. The boundary conditions, i.e. the continuity of tangential electric and magnetic field, should be satisfied and thus the decomposition coefficients of the adjacent shells are related as

TE mode:

$$u_l(k_{n-1}r_n)A_{lm}^{E}(n-1)+w_l(k_{n-1}r_n)B_{lm}^{E}(n-1)=u_l(k_nr_n)A_{lm}^{E}(n)+w_l(k_nr_n)B_{lm}^{E}(n) \quad \text{(A3)}$$

$$u'_l(k_{n-1}r_n)A_{lm}^{E}(n-1)+w'_l(k_{n-1}r_n)B_{lm}^{E}(n-1)=u'_l(k_nr_n)A_{lm}^{E}(n)+w'_l(k_nr_n)B_{lm}^{E}(n) \quad \text{(A4)}$$

TM mode:

$$u_l(k_{n-1}r_n)A_{lm}^{M}(n-1)+w_l(k_{n-1}r_n)B_{lm}^{M}(n-1)=u_l(k_nr_n)A_{lm}^{M}(n)+w_l(k_nr_n)B_{lm}^{M}(n) \quad \text{(A5)}$$

$$u'_l(k_{n-1}r_n)A_{lm}^{M}(n-1)+w'_l(k_{n-1}r_n)B_{lm}^{M}(n-1)=\frac{\varepsilon_{n-1}}{\varepsilon_n}\left[u'_l(k_nr_n)A_{lm}^{M}(n)+w'_l(k_nr_n)B_{lm}^{M}(n)\right] \quad \text{(A6)}$$

where $u_l(kr)\equiv rj_l(kr)$ and $w_l(kr)\equiv rh_l^{(1)}(kr)$. The prime denotes the derivative d/dr. One then obtains

#82976 - $15.00 USD Received 11 May 2007; revised 18 May 2007; accepted 18 May 2007; published 24 May 2007

$$\begin{pmatrix} A_{lm}^{E/M}(n-1) \\ B_{lm}^{E/M}(n-1) \end{pmatrix} = \begin{bmatrix} M_{l,11}^{E/M}(n) & M_{l,12}^{E/M}(n) \\ M_{l,21}^{E/M}(n) & M_{l,22}^{E/M}(n) \end{bmatrix} \begin{pmatrix} A_{lm}^{E/M}(n) \\ B_{lm}^{E/M}(n) \end{pmatrix} \tag{A7}$$

where the matrix element $M_{l,ij}^{E/M}(n)$ (i,j = 1,2) can be readily obtained from Eqs. (A3)-(A6). By using Eq. (A7) recursively, one obtains

$$\begin{pmatrix} A_{lm}^{E/M}(0) \\ B_{lm}^{E/M}(0) \end{pmatrix} = \begin{bmatrix} H_{l,11}^{E/M} & H_{l,12}^{E/M} \\ H_{l,21}^{E/M}(n) & H_{l,22}^{E/M} \end{bmatrix} \begin{pmatrix} A_{lm}^{E/M}(P) \\ B_{lm}^{E/M}(P) \end{pmatrix} \tag{A8}.$$

Since there is no inward going wave in the outer most medium, i.e. $A_{lm}^{E/M}(P)=0$, the outward total reflection coefficient and transmission coefficient are obtained as

$$R_{out,l}^{E/M} = H_{l,12}^{E/M} / H_{l,22}^{E/M} \tag{A9}$$

$$T_{out,l}^{E,M} = 1/H_{l,22}^{E/M} \tag{A10}.$$

The total reflection coefficient of the inner shells is calculated similarly by using the condition $B_{lm}^{E/M}(-Q)=0$.

With the consideration of the non-local effects due to the excitation of longitudinal plasmon modes [22-24], we now treat the case where ultra-thin metallic shells exist. In the metallic shell (for example in the nth shell), the expression for the electric field of TE mode does not change while the expression of TM mode should be modified as [27]

$$\begin{aligned} E^{TM}(\vec{r}) = & \sum_{l=1}^{\infty}\sum_{m=-l}^{l}\left(-\frac{\nabla\times\nabla\times\vec{r}\left(A_{lm}^{M}(n)\,j_l(k_n|\vec{r}|)+B_{lm}^{M}(n)\,h_l^{(1)}(k_n|\vec{r}|)\right)Y_{lm}(\theta,\phi)}{\omega\varepsilon\varepsilon_n\sqrt{l(l+1)}}\right) \\ & +\sum_{l=1}^{\infty}\sum_{m=-l}^{l}\frac{1}{\omega\varepsilon\varepsilon_n}\nabla\left[\left(C_{lm}\,j_l(k_L|\vec{r}|)+D_{lm}h_l^{(1)}(k_L|\vec{r}|)\right)Y_{lm}(\theta,\phi)\right] \end{aligned} \tag{A11}.$$

Here k_L is the longitudinal wave vector satisfying the dispersion relation $\varepsilon_L(k_L,\omega)=0$, where $\varepsilon_L(k_L,\omega)$ is the nonlocal longitudinal dielectric function [22]. According to the hydrodynamic model, dielectric functions of metal for the transverse and longitudinal modes are given by

$$\varepsilon(\omega) = 1-\frac{\omega_p^2}{\omega^2+i\omega\gamma} \tag{A12}$$

$$\varepsilon_L(k_L,\omega) = 1-\frac{\omega_p^2}{\omega^2-0.6v_f^2k_L^2+i\omega\gamma} \tag{A13}$$

where v_f , ω_p and γ are the Fermi velocity, plasma angular frequency and a damping coefficient, respectively. In the case of silver, the Fermi velocity is 1.39×10^8 cm/s. In order to describe the optical properties of a real metal (silver), we have chosen the following procedure as in Ref. [24]: at each angular frequency, according to Eq. (A12) first we obtain ω_p and γ by using the dielectric constant of silver [32] at the same frequency and then calculate k_L from Eq. (A13). For boundary conditions, besides the continuity of the tangential components of the electric and magnetic fields, an additional boundary condition, i.e. the continuity of the normal component of the electric field [22], is required. Assuming that the ultrathin metal

#82976 - $15.00 USD Received 11 May 2007; revised 18 May 2007; accepted 18 May 2007; published 24 May 2007

shell (n^{th} layer) is sandwiched between two ordinary shells, the decomposition coefficients of the adjacent shells are related by

$$u_l(k_{n-1}r_n)A_{lm}^M(n-1)+w_l(k_{n-1}r_n)B_{lm}^M(n-1)=u_l(k_nr_n)A_{lm}^M(n)+w_l(k_nr_n)B_{lm}^M(n) \quad \text{(A14)}$$

$$\frac{1}{\varepsilon_{n-1}}\left[u'_l(k_{n-1}r_n)A_{lm}^M(n-1)+w'_l(k_{n-1}r_n)B_{lm}^M(n-1)\right]=\frac{1}{\varepsilon_n}\left[u'_l(k_nr_n)A_{lm}^M(n)+w'_l(k_nr_n)B_{lm}^M(n)\right] \quad \text{(A15)}$$
$$-\frac{i\sqrt{l(l+1)}}{\varepsilon_n}\left[j_l(k_Lr_n)C_{lm}+h_l^{(1)}(k_Lr_n)D_{lm}\right]$$

$$\frac{\sqrt{l(l+1)}}{\varepsilon_{n-1}r_n}\left[A_{lm}^M(n-1)j_l(k_{n-1}r_n)+B_{lm}^M(n-1)h_l^{(1)}(k_{n-1}r_n)\right]=\frac{\sqrt{l(l+1)}}{\varepsilon_nr_n}\left[A_{lm}^M(n)j_l(k_nr_n)+B_{lm}^M(n)h_l^{(1)}(k_nr_n)\right] \quad \text{(A16)}$$
$$-\frac{i}{\varepsilon_n}\left[j'_l(k_Lr_n)C_{lm}+h'^{(1)}_l(k_Lr_n)D_{lm}\right]$$

$$u_l(k_{n+1}r_{n+1})A_{lm}^M(n+1)+w_l(k_{n+1}r_{n+1})B_{lm}^M(n+1)=u_l(k_nr_{n+1})A_{lm}^M(n)+w_l(k_nr_{n+1})B_{lm}^M(n) \quad \text{(A17)}$$

$$\frac{1}{\varepsilon_{n+1}}\left[u'_l(k_{n+1}r_{n+1})A_{lm}^M(n+1)+w'_l(k_{n+1}r_{n+1})B_{lm}^M(n+1)\right]=\frac{1}{\varepsilon_n}\left[u'_l(k_nr_{n+1})A_{lm}^M(n)+w'_l(k_nr_{n+1})B_{lm}^M(n)\right] \quad \text{(A18)}$$
$$-\frac{i\sqrt{l(l+1)}}{\varepsilon_n}\left[j_l(k_Lr_{n+1})C_{lm}+h_l^{(1)}(k_Lr_{n+1})D_{lm}\right]$$

$$\frac{\sqrt{l(l+1)}}{\varepsilon_{n+1}r_{n+1}}\left[A_{lm}^M(n+1)j_l(k_{n+1}r_{n+1})+B_{lm}^M(n+1)h_l^{(1)}(k_{n+1}r_{n+1})\right]=\frac{\sqrt{l(l+1)}}{\varepsilon_nr_{n+1}}\left[A_{lm}^M(n)j_l(k_nr_{n+1})+B_{lm}^M(n)h_l^{(1)}(k_nr_{n+1})\right] \quad \text{(A19)}$$
$$-\frac{i}{\varepsilon_n}\left[j'_l(k_Lr_{n+1})C_{lm}+h'^{(1)}_l(k_Lr_{n+1})D_{lm}\right]$$

By using the above equations, one can obtain

$$\begin{pmatrix}A_{lm}^M(n-1)\\B_{lm}^M(n-1)\end{pmatrix}=\begin{bmatrix}M_{l,11}^M(n) & M_{l,12}^M(n)\\M_{l,21}^M(n) & M_{l,22}^M(n)\end{bmatrix}\begin{pmatrix}A_{lm}^M(n+1)\\B_{lm}^M(n+1)\end{pmatrix} \quad \text{(A.20)}$$

Thus one can also obtain Eq. (A8) by applying Eq. (A7) or Eq. (A20) recursively. The total reflection coefficients and transmission coefficient are calculated in the same way.

#82976 - $15.00 USD Received 11 May 2007; revised 18 May 2007; accepted 18 May 2007; published 24 May 2007